Supporting Information

Ganguly et al. 10.1073/pnas.1606610113

SI Materials and Methods

MD Simulations. The starting structures of the MD simulations were based on the crystal coordinates of full-length *Drosophila* cryptochrome (PDB ID code 4GU5) (6, 7). The protonation states of the nonactive site histidine residues were determined from visual inspection of hydrogen bonding networks. Surface exposed His residues were assumed to be neutral. dCRY was immersed in an orthorhombic box of rigid 3-site transferable intermolecular potential (TIP3P) waters, and Na^+ and Cl^- ions were added to produce a neutral physiological salt concentration of 0.15 M (23). The solvated box was replicated in all three dimensions using periodic boundary conditions and long-range electrostatic interactions were calculated using the particle mesh Ewald (PME) method (24) with a cutoff of 12 Å. Bonds involving hydrogen were constrained by the SHAKE algorithm (25). After equilibrating the system through several stages that held either pressure (P) or volume (V) constant and varied temperature (T), production trajectories of 25 ns were computed at 298 K in the canonical ensemble of N particles (i.e., constant NVT) with a 1-fs time step. A modified Nosé–Hoover method in conjunction with Langevin dynamics was used to maintain constant pressure and temperature during the simulations. Additional details regarding the equilibration protocol are provided below. All MD simulations were performed using the NAMD program (26) using the CHARMM22 force field (27) with the CMAP correction (28).

MD simulations were performed with two redox states of the flavin [the neutral state (FAD) and the ASQ state (FAD^{-})] and three protonation states of the active site His378 residue (protonated at the N1 position, protonated at the N3 position, and protonated at both N1 and N3 positions). In total, we computed MD trajectories for six scenarios, corresponding to all combinations of the above-mentioned flavin redox states and His378 protonation states. For each scenario, we propagated three independent MD trajectories. The charges of the neutral flavin molecule were taken from a previous study (29). Those of the negatively charged flavin were obtained in a similar fashion by fitting the electrostatic potential from ab initio quantum mechanical calculations onto the negatively charged flavin molecule while taking the charges of the neutral flavin as an initial guess.

Equilibration protocol used in the MD simulations:

In each MD simulation, the following steps of equilibration were performed before the production run was propagated.

i) Energy minimization of the solvent (water, Na^+, and Cl^- ions) with the protein fixed at its crystal coordinates.
ii) Optimization of only the protein hydrogen atoms with the protein heavy atoms and solvent fixed.
iii) MD at 298 K at constant NPT for 100 ps with the protein fixed.
iv) Simulated annealing of both protein and solvent at constant NPT.
  a) Increase temperature from 0 to 100 K in 10 ps.
  b) MD at 100 K for 100 ps.
  c) Increase temperature from 100 to 200 K in 10 ps.
  d) MD at 200 K for 100 ps.
  e) Increase temperature from 200 to 298 K in 10 ps.
  f) MD at 298 K for 500 ps.
v) MD at 298 K at constant NVT for 1 ns.

PCA. PCA involves the calculation of the covariance matrix of the system during an MD simulation, which is given by

$$C_{ij} = \langle (x_i - \langle x_i \rangle)(x_j - \langle x_j \rangle) \rangle,$$

where $x_1, x_2, \ldots, x_{3N}$ are the mass-weighted Cartesian coordinates of an N-particle system and $\langle\ \rangle$ denotes the average over the MD simulation. The symmetric $3N \times 3N$ matrix C can be diagonalized to obtain a set of eigenvectors, or the principal modes of the trajectory

$$R^T C R = diag(\lambda_1, \lambda_2, \ldots, \lambda_{3N}),$$

where R is a transformation matrix containing the eigenvectors and $(\lambda_1 > \lambda_2 > \lambda_{3N})$ are the corresponding eigenvalues. The principal components of the trajectory $q_i(t), i = 1, \ldots, 3N$, are obtained by projecting the trajectory onto the eigenvectors. They describe the directions of collective motions, whereas the corresponding eigenvalues measure the mean-square fluctuation of the trajectory in those directions. Typically, only the first few principal components are important because they define the dominant collective motions in the system.

We performed a PCA on the motions of the FFW motif residing in the dCRY CTT. Rotational and translational motions from the MD trajectories were removed by first calculating root mean squared fluctuations (RMSFs) of all residues from each independent MD trajectory after aligning each trajectory to the protein backbone of the crystal structure. The average RMSFs of each residue from all of the MD trajectories were calculated, and each trajectory was realigned based on only those residues that had average RMSFs below a threshold of 1.3 Å. The coordinates of the atoms corresponding to the FFW motif were extracted from these various aligned trajectories and concatenated into a single trajectory on which the PCA was performed.

To explore correlated motions in dCRY, we constructed dynamic cross-correlation matrixes (DCCMs) for all MD trajectories. The DCCM of a trajectory was generated by normalizing the covariance matrix of the entire trajectory according to

$$C_{ij}^{corr} = C_{ij} / \sqrt{C_{ii} C_{jj}}.$$

The DCCMs were generated for coarse-grained trajectories where each residue from the atomistic MD trajectories was replaced with a particle at its center of mass. All analyses related to PCA and DCCMs were performed using GROMACS tools, namely trjconv, g_covar, and g_anaeig (30).

pK_a Calculations with the PB/LRA. The PB/LRA approach allows the estimation of the shift in the pK_a of a residue in its protein environment with respect to its pK_a in solution. Within the PB approach, the shift in the pK_a of a residue AH is expressed as the difference between the electrostatic deprotonation free energies of the residue in the protein environment and in aqueous solution, and is calculated as

$$\Delta pK_a = \Delta\Delta G / 2.303RT,$$

where $\Delta\Delta G = [(G_A^{protein} - G_{AH+}^{protein}) - (G_A^{aq} - G_{AH+}^{aq})]$, R is the gas constant, *protein* denotes the protein environment, and *aq* denotes aqueous solution (31–33). In these calculations, the solvated protein is represented as a medium of low dielectric constant with partial point charges at the atomic positions, surrounded by implicit solvent with a high dielectric constant (~80). The choice of the internal protein dielectric constant, $\epsilon_{protein}$, typically ranges from 2 to 8 (34). An established approach to

account for protein environment relaxation is to compute MD trajectories and calculate the average ΔpK_a for several snapshots along these MD trajectories (19). In the LRA framework, independent MD trajectories with protonated and deprotonated forms of the residue of interest in the protein environment are generated, and the final pK_a shift is calculated by averaging over the snapshots obtained from both trajectories. Previous studies have shown this approach to be effective in reproducing experimentally measured pK_a shifts in proteins and RNAs (19).

In this study, we used the PB/LRA approach to estimate the pK_a shifts of His378 at the N1 and N3 positions caused by the reduction of the flavin. We calculated the pK_as of His378 in the protein environment relative to the pK_a of an isolated His378 in aqueous solution for both FAD and FAD^{-} states of the flavin. The calculations were performed on snapshots generated from the various MD trajectories described earlier in the section. Each pK_a value was obtained by averaging over PB calculations on 250 configurations extracted from the respective 25-ns-long MD trajectories at equal intervals. The results in Table S1 were obtained using a $\epsilon_{protein} = 2$, whereas calculations with $\epsilon_{protein} = 4$ (Table S2) gave quantitatively similar results. As a consistency check, we performed three independent pK_a calculations using snapshots from three independent trajectories.

REMD Simulations. Given the high computational expense of the REMD simulations, we explored only three scenarios that appeared to be most relevant for dCRY photoactivation as suggested by the preceding MD simulations. These scenarios are as follows: (*i*) the active site flavin is neutral and His378 is protonated at the N3 position, (*ii*) the active site flavin is negatively charged and His378 is protonated at the N3 position, and (*iii*) the active site flavin is negatively charged and His378 is protonated at both N1 and N3 positions.

In the REMD simulations, 48 replicas were distributed between 300 and 350 K. The temperatures of the replicas were chosen to be exponentially increasing to obtain uniform acceptance ratios between neighboring replicas. Each replica was equilibrated independently at its respective temperature; first under constant NVT conditions and then under constant NPT conditions for a total of 600 ps. Production trajectories were propagated under constant NPT conditions for 50 ns with a 2-fs time step. As in the traditional MD simulations, all bonds involving hydrogen were constrained using the SHAKE algorithm (25), long-range electrostatics were treated using PME (24) with a 12-Å cutoff, and a combination of a modified Nosé–Hoover method and Langevin dynamics was used to maintain constant temperature and pressure. Replica exchanges were attempted every 0.4 ps, which resulted in exchange probabilities between neighboring replicas of 20–30%. The REMD simulations were performed using the GROMACS software (30) and the CHARMM22 force field with the CMAP correction (28).

Alchemical FEP Simulations. To support the results obtained from the PB/LRA calculations, we used the FEP approach to calculate the pK_a shifts of His378 at the N1 and N3 positions triggered by the reduction of the flavin. In the FEP framework, the change in free energy of a system transforming from state A to state B is calculated according to the equation

$$\Delta G_{A\to B} = -k_B T \ln\langle \exp(-\{U_B - U_A\}/k_B T)\rangle_A,$$

where k_B is the Boltzmann constant, and T is the absolute temperature. U_B and U_A are the potential energies of states B and A, respectively, and $\langle ... \rangle_A$ indicates an ensemble average over configurations sampled with the system in state A. Because the two final states are often quite different, in practice the transformation is achieved by summing over a series of smaller transformations between nonphysical, intermediate states connecting the two final states along a path characterized by a coupling parameter, λ (35)

$$\Delta G_{A\to B} = -k_B T \sum_i^N \ln\langle \exp(-\{U_{\lambda_i+1} - U_{\lambda_i}\}/k_B T)\rangle_i.$$

The FEP simulations in this study are performed within the dual-topology framework (36), in which the total number of atoms in the system is divided into three groups: atoms specific to state A, atoms specific to state B, and atoms that are common to both the end states and do not change over the course of the simulation. The topologies corresponding to the two end states coexist but never interact. At the start of the simulation atoms specific to state A interact with the rest of the system, whereas the interactions of atoms specific to state B are switched off. During the simulation the interactions of the atoms belonging to state A are smoothly diminished, whereas interactions of the atoms belonging to state B are introduced according to λ. At the end of the simulation, the interactions of the atoms belonging to state A are completely switched off, and only atoms belonging to state B interact with the rest of the system.

We performed separate FEP simulations to calculate the free energies of deprotonation at N1 and N3 positions of His378 in presence of neutral and reduced flavin. To calculate the deprotonation at N1 position, we considered the alchemical transformation of His378 from His-DP state to His-N3P state, and to calculate the deprotonation at N3 position, we considered the alchemical transformation of His378 from His-DP state to His-N1P state. The simulations were performed in a cubic box and to account for the self-interaction energies arising due to the introduction of a charge in the system, a correction term of $1/2(-2.837297/L)$ (37), where L is the length of the box, was considered. The remaining details related to the setup of the simulations are similar to the other MD simulations performed in this study. In each FEP simulation, 50 windows were considered and in each window 25 ps of equilibration and 75 ps of production MD were performed resulting in a total simulation length of 5 ns. Each simulation was run both in the forward and reverse directions and the results were combined using the Bennett Acceptance Ratio (BAR) algorithm (38). We performed two independent FEP simulations for each case. The simulations were performed using the NAMD program (26), and the BAR estimator available within the VMD software (39) was used to combine the results from the forward and reverse FEP simulations. We note that the FEP method, while being a mathematically exact and well-established technique for estimating free energy differences between two states, is known to suffer from convergence issues. The difficulties in converging FEP simulations with medium to large perturbations has been extensively discussed in the literature (35), and thus care should be taken when interpreting results.

dCRY Expression and Purification. dCRY was cloned from constructs previously used to express in insect cells (6) and inserted into pET28a between the NdeI and XhoI restriction sites. The plasmid was expressed in CmpX13 cells containing the riboflavin importer (40) under kanamycin resistance. The cells were grown until an optical density of A600 ~0.8, induced with 4 mM isopropyl β-D-1 thiogalactopyranoside (IPTG), supplemented with 5 μM FAD, and grown overnight at room temperature (~25 °C). Cells were harvested and frozen at −80 °C.

For purification, cells were lysed by sonication in lysis buffer containing 50 mM Hepes, pH 8, 150 mM NaCl, 0.5 mM Triton-X, 0.5 mM tris(2-carboxyethyl) phosphine (TCEP), and 5 mM imidazole. Insoluble cell debris was removed by centrifugation at 48,384 × *g* for 35 min. The clarified cell lysate was applied to a Ni-NTA agarose beads (Gold Biotechnology) equilibrated with lysis

buffer, and the protein was eluted with elution buffer 50 mM Hepes, pH 8, 150 mM NaCl, 200 mM imidazole, 0.5 mM TCEP, and 10% (vol/vol) glycerol. Protein was further purified by anion exchange chromatography and Superdex 200 gel filtration column with 50 mM Hepes, pH 8.0, 10% glycerol, and 150 mM NaCl. Purified protein was used fresh after purification or flash frozen in liquid nitrogen and stored at −80 °C. Point mutations were made with Quikchange (Agilent) and confirmed by DNA sequencing (Cornell Biotechnology Center).

Spectroscopy and Kinetics. UV/Vis spectra were collected using a quartz cuvette with path length of 1 cm. All spectra were normalized by subtracting the absorbance at 800 nm. Photoreduced species of dCRY were monitored by irradiating dark-state samples with 448-nm diode laser light (30 mW; World Star Tech) perpendicular to the observation beam. Full spectra were collected on an Agilent 8453 diode-array spectrophotometer as a function of time. In kinetics mode, data were obtained by monitoring samples at 365, 403, and 450 nm with a cycle time of 1.0 s under temperature control. Traces for gains in the ASQ at 365 nm were fit with MATLAB (The MathWorks) to

$$y(t) = A\left(1-e^{-k_1(t-t_0)}\right)+B\left(1-e^{-k_2(t-t_0)}\right)+y_0, \qquad \textbf{[S1]}$$

where A, B, and y_0 are coefficients, t_0 is the x axis offset, and k_1 and k_2 are rate constants. Traces were mostly monoexponential, but in most cases were better fit to a biexponential function. Only the pH dependence of the major phase, which represents >95% of the amplitude was considered. The pH dependence of the WT was fit to a simple model that assumes a single deprotonation event

$$k_{obs} = \frac{k_{HA}[H^+]+k_A K_A}{K_A+[H^+]}, \qquad \textbf{[2]}$$

where k_{HA} is the rate constant for the protonated base, k_A is the rate constant for the deprotonated form, and K_A is the acid dissociation constant.

Proteolytic Sensitivity Assay. Ten microliters of 35.4 μM CRY was added to 3 μL 4.2 μM trypsin (bovine pancreatic; Sigma-Aldrich) and quenched after 30 s with 3 μL 8.4 μM trypsin inhibitor (soybean; Sigma-Aldrich). The sample was then mixed with 5 μL lithium dodecyl sulfate loading buffer (4×; ThermoFisher) and heated at 90 °C for 10 min, and a 5-μL aliquot was visualized on SDS/PAGE with Coomassie blue staining. For the light-state samples, CRY was exposed to 448-nm laser light (30 mW; World Star) after passing through a neutral density filter (OD = 1; ND510B; Thor Labs) for various times before addition of trypsin. The sample was kept under light for the 30-s digestion period. An emerging band that represents cleavage of the CTT (~50 kDa; band II) (10) was followed as a function of light exposure and quantified on gel scans with ImageJ (NIH). Band intensities were compared with those after full exposure under unfiltered light for 8 min.

Cell Culture Stability Assays. dCRY, *Drosophila* ls-TIM (dTIM; long and short allele), and *Drosophila* Jetlag (JET), or site-directed mutants thereof, were N-terminally tagged with three myc epitopes, C-terminally tagged with three hemagglutinin (HA) epitopes, or C-terminally tagged with a FLAG epitope, respectively, and cloned into the pAc5.1/V5 vector (Invitrogen) using standard cloning protocols. S2 cells were grown in Schneider's medium supplemented with 10% (wt/vol) FBS and penicillin/streptomycin. dCRY was cotransfected with either empty vector or dTIM + JET plasmid with effectene (Qiagen) using the manufacturer's protocols. Cell medium was refreshed after 24 h in the transfection mixture, and the cells were divided into two populations. Twenty-four hours later, each population was lysed in a modified radio immunoprecipitation buffer under red light or after being exposed to white light for 1 h (~600 lx). Equal amounts of lysates were run on 6% (wt/vol) SDS/PAGE gels and immunostained using myc (Sigma), HA (Roche), anti-FLAG (Sigma), and tubulin (Sigma) antibodies. Tubulin was used as a loading control. Transfections were performed in triplicate, and each triplicate was repeated at least twice with similar results.

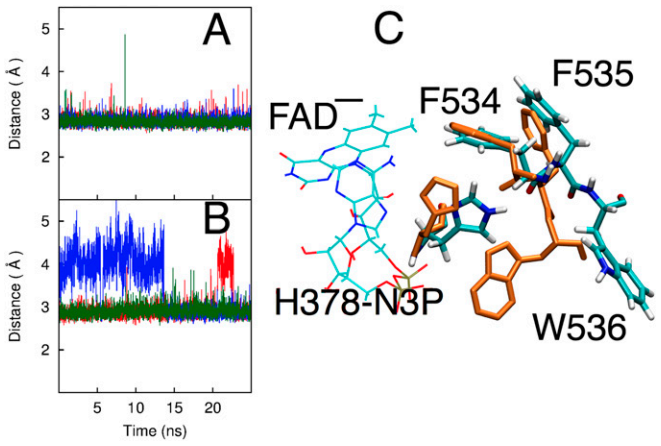

Fig. S1. Comparison of the active site conformations between simulations with His378 protonated at the N3 position, in the presence of oxidized FAD (*A*) and reduced FAD (*B*). In *A* and *B*, the FAD(OS2)–His378(N1) distance is plotted along the respective MD trajectories. (*C*) Representative snapshot of the active site from FAD⁻:His-N3P simulations in which His378 is pushed toward the CTT resulting in the CTT release. The crystal conformation of His378 and the CTT is shown in orange for comparison.

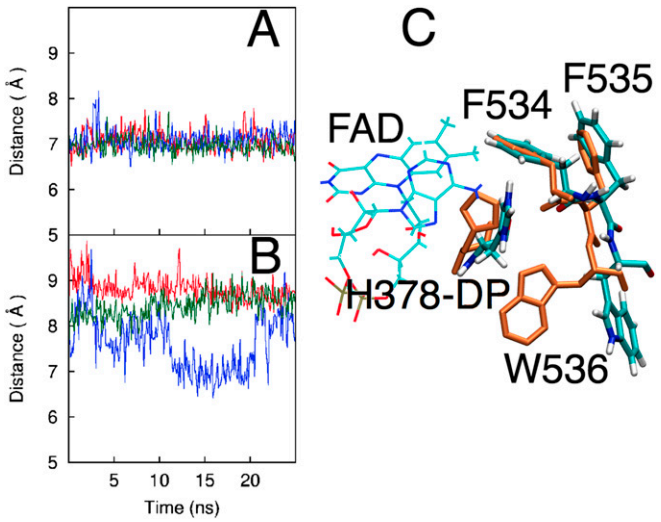

Fig. S2. Comparison of the active site conformations between simulations with His378 protonated at both the N1 and N3 positions in the presence of neutral FAD (*A*) and in the presence of reduced FAD (*B*). In *A* and *B*, the FAD isoalloxazine ring center of mass – His378 imidazole ring center of mass distance is plotted along the respective MD trajectories. (*C*) Representative snapshot of the active site from FAD^{-}:His-DP simulations in which His378 is pushed toward the CTT, resulting in the CTT release. The crystal conformation of His378 and the CTT is shown in orange for comparison.

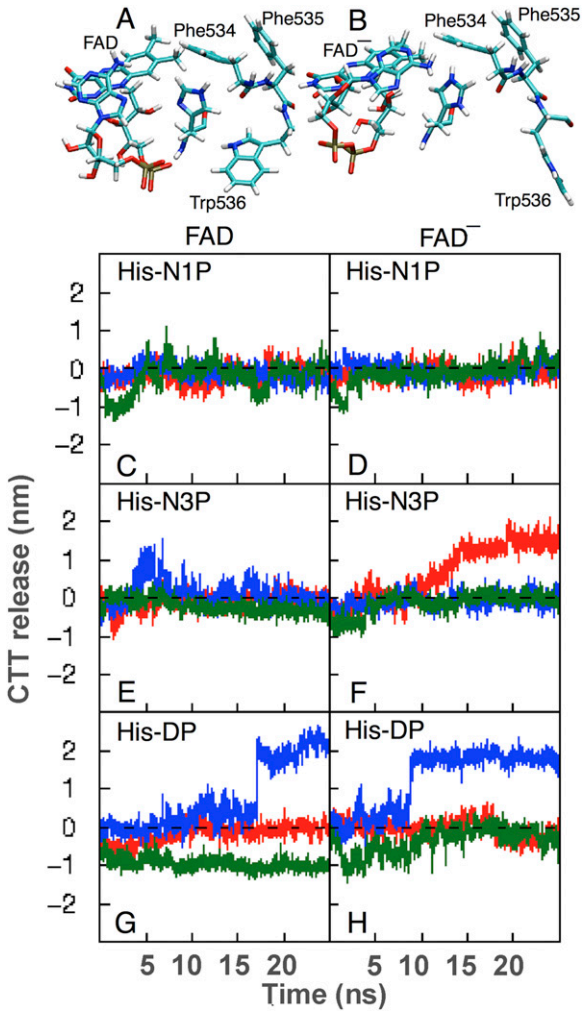

Fig. S3. CTT release of dCRY. Representative snapshots of the dCRY active site are shown with the CTT in closed (*A*) and open (*B*) conformations. The first PCA mode that corresponds to the CTT opening is plotted along the trajectories from the MD simulations with FAD oxidized and His378 N1 protonated (*C*), FAD reduced and His378 N1 protonated (*D*), FAD oxidized and His378 N3 protonated (*E*), FAD reduced and His378 N3 protonated (*F*), FAD oxidized and His378 protonated at both N1 and N3 (*G*), and FAD reduced and His378 protonated at both N1 and N3 (*H*). The red, blue, and green colors correspond to three independent trajectories. As evident from the sudden transitions of the respective PCA modes from negative or neutral to positive values, CTT release was observed in three cases: in two cases FAD is reduced, with His-3P (*F*) and His-DP (*H*), and in a third case FAD is oxidized with His-DP (*G*). *F–H* are reproduced form Fig. 2 to aid comparison.

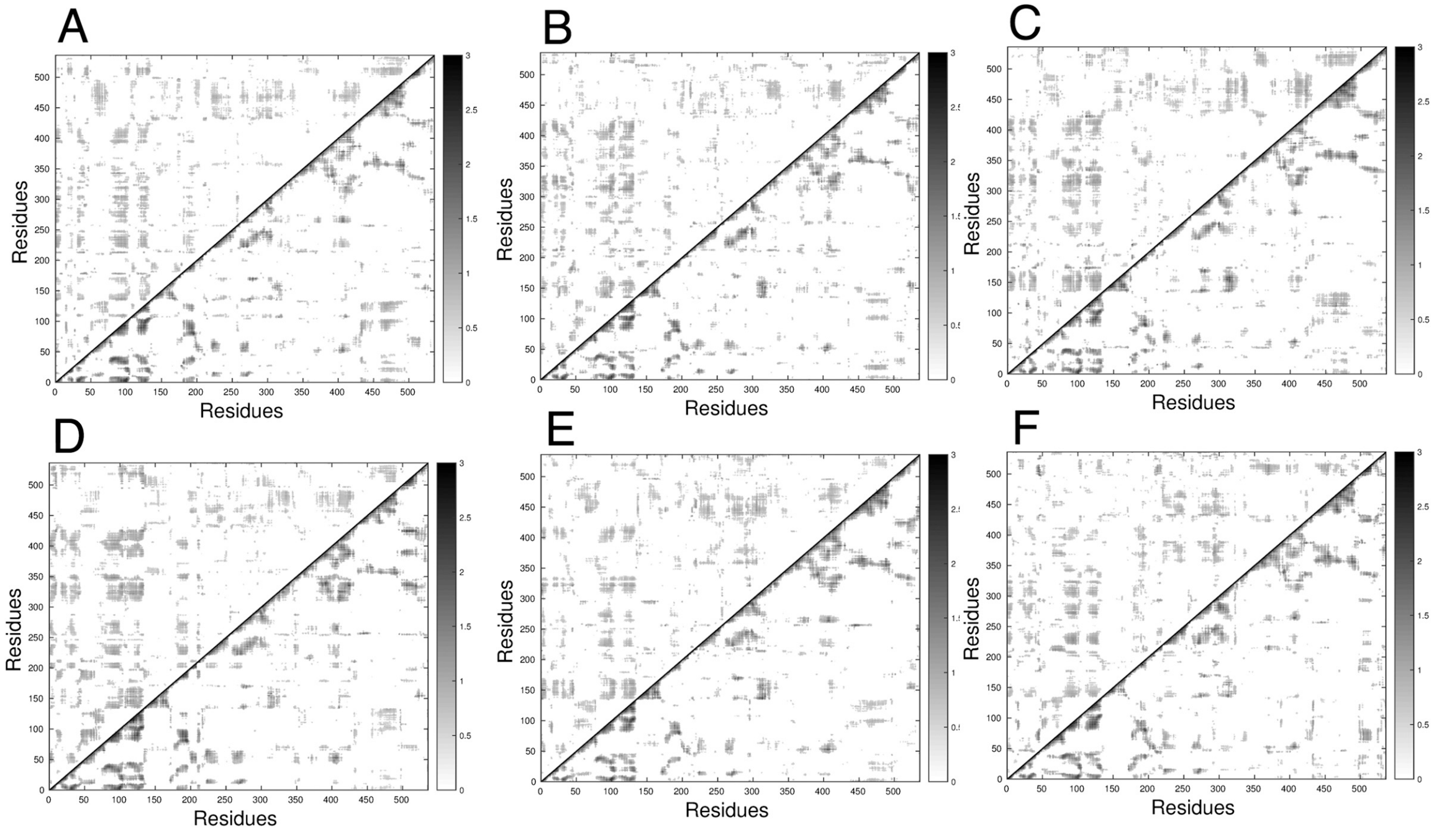

Fig. S4. Correlated motions in dCRY. (*A*–*F*) DCCMs constructed from MD simulations with FAD oxidized and His378 N1 protonated (*A*; Fig. S3*C*), FAD oxidized and His378 N3 protonated (*B*; Fig. S3*E*), FAD oxidized and His378 protonated at both N1 and N3 (*C*; Fig. S3*G*), FAD reduced and His378 N1 protonated (*D*; Fig. S3*D*), FAD reduced and His378 protonated at N3 (*E*; Fig. S3*F*), and FAD reduced and His378 protonated at both N1 and N3 (*F*; Fig. S3H). Each DCCM was constructed from a respective single independent MD trajectory. The calculations were repeated with other independent trajectories and the results were qualitatively similar.

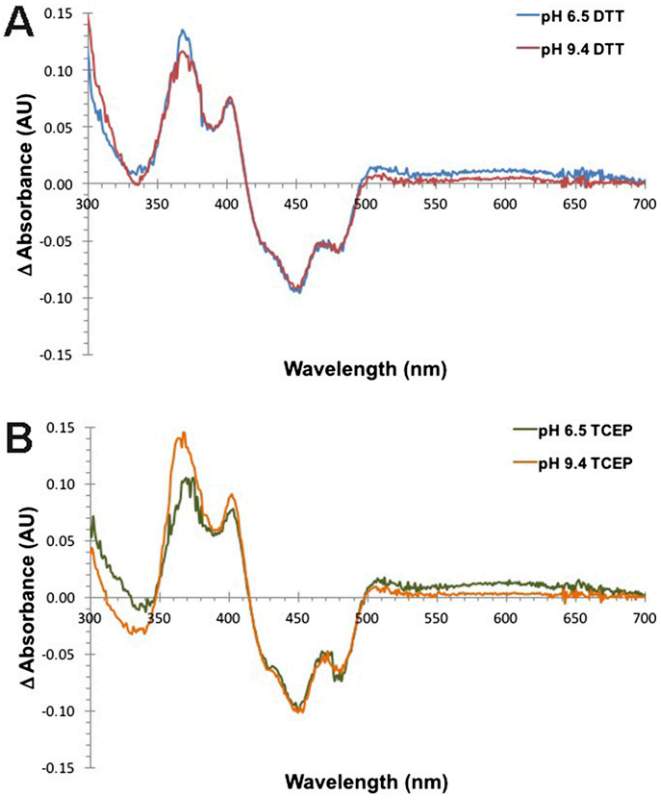

Fig. S5. pH-dependent neutral semiquinone formation in dCRY. Difference spectra of dCRY in the fully photoreduced state and the oxidized state show a small amount of neutral semiquinone formation at pH 6.5, but virtually none at pH 9.4, as evidenced by the broad absorption band at 610 nm. Results were similar for two reductive quenchers: (*A*) DTT and (*B*) TCEP.

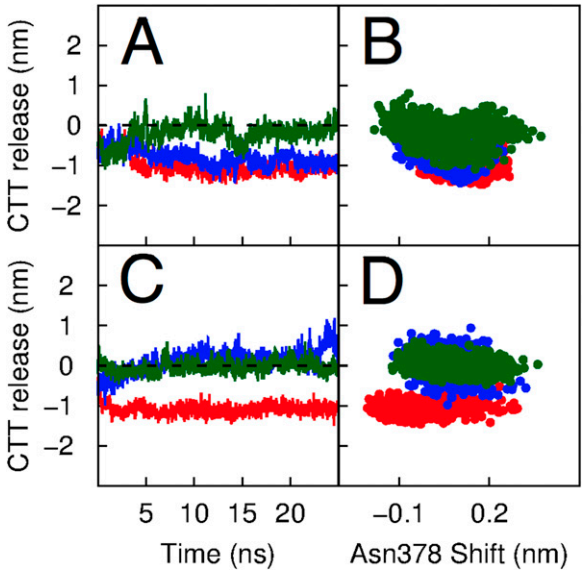

Fig. S6. MD simulation results from the His378Asn variant. (*A* and *C*) CTT opening over the course of the reaction, as depicted in Fig. 2 (*A*, FAD; *C*, FAD^{-}). *B* and *D* correlate the Asn378 shift with the CTT release measured against the first PCA mode, as in Fig. 3 (*B*, FAD; *D*, FAD^{-}).

Table S1. ΔG(closed → open) states calculated from REMD simulations

Case	Total CTT release	Open	Closed	Δ*G* (kcal/mol)
FAD:His-N3P	9,813	1,998	7,815	0.80
FAD^{-}:His-N3P	8,976	4,776	4,200	−0.08
FAD^{-}:His-DP	8,859	5,750	3,109	−0.36

ΔG(closed →open) is expressed as $-kT\ln(P_{open}/P_{closed})$, where P_{open} and P_{closed} are the probabilities of open and closed states, respectively, k_B is the Boltzmann constant and T is the absolute temperature.

Table S2. pK_a values of His378 from PB/LRA calculations, $\varepsilon_{protein} = 2$

Site	Independent calculations	Flavin state	ΔΔ*G*	ΔpK_a	*p*K_a shift
N1	1	FAD	−14.9 (0.6)	−10.8	0
		FAD^{-}	−14.9 (0.5)	−10.8	
	2	FAD	−9.3 (0.3)	−6.7	0.5
		FAD^{-}	−8.5 (0.1)	−6.2	
	3	FAD	−15.3 (0.6)	−11.2	2.7
		FAD^{-}	−11.6 (0.5)	−8.5	
N3	1	FAD	−10.0 (0.5)	−7.2	4.0
		FAD^{-}	−4.4 (0.5)	−3.2	
	2	FAD	−10.9 (0.4)	−7.9	3.2
		FAD^{-}	−6.4 (0.5)	−4.7	
	3	FAD	−9.2 (0.4)	−6.7	4.7
		FAD^{-}	−2.8 (0.6)	−2.0	

ΔΔG values represent the change in free energy for deprotonating the given nitrogen from the doubly protonated state in the protein environment compared with solution (SDs in parentheses). $\Delta\Delta G = 1.38\ \Delta pK_a$.

Table S3. pK_a values of His378 from PB/LRA calculations, $\varepsilon_{protein} = 4$

Site	Independent calculations	Flavin state	ΔΔ*G*	ΔpK_a	*p*K_a shift
N1	1	FAD	−7.9 (0.3)	−5.7	0.2
		FAD^{-}	−7.6 (0.2)	−5.5	
	2	FAD	−9.8 (0.2)	−7.1	3.5
		FAD^{-}	−4.9 (0.1)	−3.6	
	3	FAD	−8.4 (0.3)	−6.1	−1.4
		FAD^{-}	−10.3 (0.6)	−7.5	
N3	1	FAD	−5.6 (0.2)	−4.1	2.4
		FAD^{-}	−2.3 (0.3)	−1.7	
	2	FAD	−6.4 (0.2)	−4.6	2.4
		FAD^{-}	−3.1 (0.3)	−2.2	
	3	FAD	−4.8 (0.2)	−3.5	2.4
		FAD^{-}	−1.5 (0.4)	−1.1	

See legend of Table S2.

Table S4. pK_a values of His378 from FEP calculations

Site	Independent calculations	Flavin state	ΔG	ΔpK_a	pK_a shift
N1	1	FAD	25.6 (0.2)	18.6	6.9
		FAD^-	35.2 (0.2)	25.5	
	2	FAD	24.7 (0.1)	17.9	6.9
		FAD^-	34.2 (0.1)	24.8	
N3	1	FAD	33.0 (0.2)	23.9	2.1
		FAD^-	35.9 (0.1)	26.0	
	2	FAD	33.4 (0.2)	24.2	2.8
		FAD^-	37.3 (0.1)	27.0	

ΔG values represent the change in free energy for deprotonating the given nitrogen from the doubly protonated state in the protein environment. The numbers in parentheses are statistical errors obtained from the combination of the forward and reverse FEP simulations using the BAR method (23). $\Delta\Delta G = 1.38\ \Delta pK_a$.

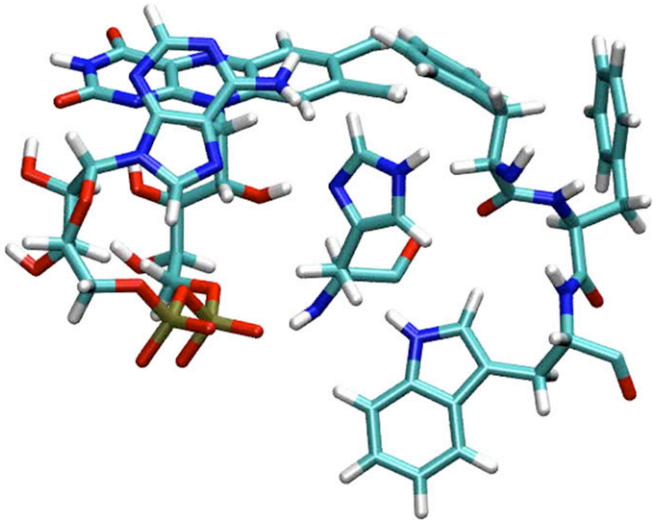

Movie S1. FAD^-:His-N3P case. Animation of a MD trajectory with reduced flavin (FAD^-) and His378 protonated at N3 (His-N3P) where in the CTT release was observed. For clarity, only the active site, comprising of the flavin, His378, and residues 534–536 (the FFW motif) are shown in licorice representation. The MD trajectory was first aligned to the crystal structure and then to remove thermal noise the trajectory was smoothed by replacing the coordinates of each frame with the average coordinates calculated over a window of nine consecutive frames centered on that particular frame.

Movie S1

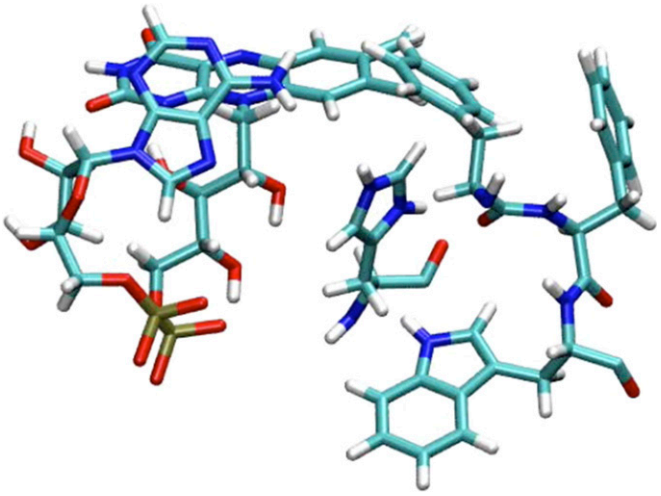

Movie S2. FAD^{-}:His-DP case. Animation of an MD trajectory with reduced flavin (FAD^{-}) and His378 protonated at both N1 and N3 (His-DP) where in the CTT release was observed. For clarity, only the active site, comprising of the flavin, His378, and residues 534–536 (the FFW motif) are shown in licorice representation. A similar aligning and smoothing of the MD trajectory was performed as in the case of Movie S1.

Movie S2

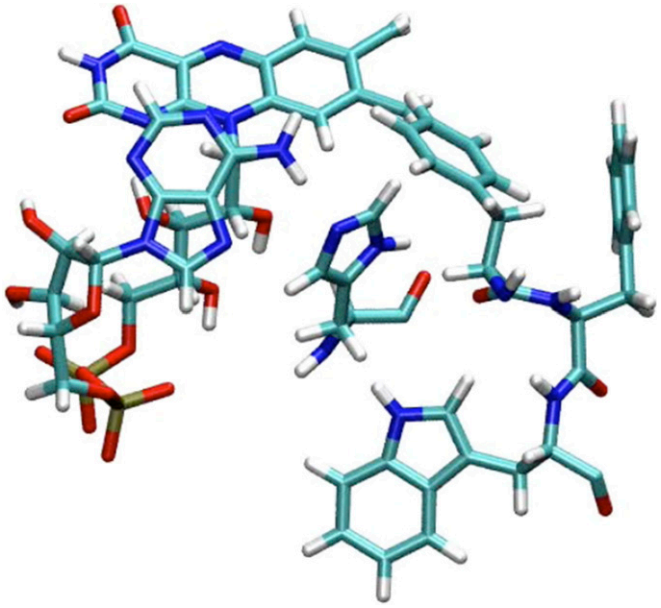

Movie S3. FAD:His-N1P case. Animation of a representative MD trajectory with oxidized flavin (FAD) and His378 protonated at N1 (His-N1P). For clarity, only the active site, comprising of the flavin, His378, and residues 534–536 (the FFW motif) are shown in licorice representation. A similar aligning and smoothing of the MD trajectory was performed as in the case of Movie S1. In these trajectories, the FFW motif remains close to the crystal conformation and the CTT release is never observed.

Movie S3